Journal of Biomechanical Science and Engineering

Vol. 1, No. 1, 2006

Simulation Study on Effects of Hematocrit on Blood Flow Properties Using Particle Method*

Ken-ichi TSUBOTA,** Shigeo WADA*** and Takami YAMAGUCHI**

**Department of Bioengineering and Robotics, Graduate School of Engineering,
Tohoku University, 6-6-01 Aoba, Sendai 980-8579, Japan
E-mail: tsubota@pfsl.mech.tohoku.ac.jp, takami@pfsl.mech.tohoku.ac.jp

***Department of Mechanical Science and Bioengineering,
Graduate School of Engineering Science, Osaka University,
1-3 Machikane-yama, Toyonaka 560-8531, Japan
E-mail: shigeo@me.es.osaka-u.ac.jp

Abstract

The effects of hematocrit (Hct) on blood flow in microcirculation were investigated by computer simulation using a particle method. Deformable red blood cells (RBCs) and blood plasma were modeled by assembly of discrete particles. It was assumed that an RBC consisted of an elastic membrane and inner viscous fluid, and that plasma was viscous fluid. The particles for the RBC membrane were connected with their neighboring membrane particles by stretch/compression and bending springs. The motion of all the particles that was subjected to incompressible viscous flow was solved by the moving particle semi-implicit (MPS) method based on Navier-Stokes (NS) equations. The forces induced by the springs to express the elastic RBC membrane were substituted into the NS equations as the external force, which enabled coupled analysis of elastic RBC motion and plasma fluid flow. Two-dimensional simulations of blood flow between parallel plates were carried out for various Hct values. As a result, it was shown that at higher Hct, RBCs were less deformed into a parachute shape during their downstream motion, indicating that mechanical interaction between RBCs restricted the RBC deformation. Mechanical interaction between RBCs had a significant influence on RBC deformation and the velocity profile of plasma flow when the Hct value was more than 0.20～0.30. Apparent blood flow resistance increased with Hct, corresponding to previously reported *in vitro* experimental results compiled to an empirical formula.

Key words: Computational Biomechanics, Microcirculation, Red Blood Cells, Deformability, Plasma Flow, Fluid-Solid Coupled Problem, Rheology

1. Introduction

Blood is a suspension of elastic red blood cells (RBCs) in viscous plasma fluid [(1)–(3)]. In microcirculation, the volumetric ratio of RBCs to whole blood, so called hematocrit (Hct), greatly affects the rheological properties of the blood [(1), (2), (4)]. Extensive *in vitro* experimental studies have been conducted to establish an empirical formula that relates blood flow resistance to Hct [(1), (2), (4)]. This phenomenon includes the mechanical factors of (1) the shape and deformation of an RBC and (2) mechanical interaction between RBCs and plasma. Furthermore, these mechanical factors lead to (3) RBC to RBC interaction via plasma fluid. Theoretical and computational approaches have been useful for understanding the role of these mechanical factors in blood flow phenomena [(2), (5)].

*Received 17 May, 2006 (No. 06-0026)
[DOI: 10.1299/jbse.1.159]

However, there is little investigation on the combined effects of these mechanical factors on blood flow depending on Hct because established numerical methods (usually with Euler grids) have not enabled the computation of these factors at the same time.

Recently, the motions of multiple RBCs have been investigated by computer mechanical simulation to explain the mechanism of how the Hct determines the rheological properties of blood in microvasculature. Sun and Munn [5] proposed the two-dimensional lattice Boltzmann method to simulate blood flow considering individual blood cells suspending in plasma. They qualitatively reproduced the motions of multiple blood cells observed in experiments, such as the axial migration of RBCs and appearance of a plasma layer near the vascular wall, and suggested that the RBC behavior determines the resulting flow resistance that depends on Hct as observed in experiments. However, they modeled RBCs as a rigid body and did not consider their deformabilities. On the other hand, Boryczko et al. [6] simulated three-dimensional blood flow in capillary including multiple RBCs using a discrete particle model, and suggested that combined effects of Hct and RBC deformation play an important role in apparent blood flow properties. However, they modeled an RBC as a solid elastic body, and the inner fluid of the RBC was ignored.

As denoted above, recent advances in computational techniques combined with increasing computing power allow us to calculate the complicated mechanical interaction among blood cells suspending in plasma. In particular, a particle method, which has been used to analyze fluid, solid and fluid-solid coupled mechanical problems [7], has begun to be applied to blood flow simulation [6], [8]–[12]. This method does not need mesh generation such as that used in the finite element method, and only uses the discrete particles as computing points that are traced in Lagrangian coordinates. The motion of each particle is determined by its mechanical interaction with neighboring particles, which is modeled to express the analyzing object. The method is advantageous in directly modeling each blood component [6], [8]–[12], such as a blood cell and plasma, using an assembly of discrete particles that are assigned the characteristic properties of the corresponding blood component. In addition, the complex mechanical/biological interaction between blood components can be expressed in the blood flow simulation by taking into account only the interaction between these particles.

The purpose of this study is to investigate the effects of Hct on blood flow properties on the blood cellular scale from the viewpoint of computational mechanics. A particle method was used to simulate two-dimensional blood flow between parallel plates, which is a simplified flow model of microcirculation. Blood was considered as a suspension of multiple RBCs, consisting of an elastic surface membrane and inner viscous fluid, in viscous fluid of blood plasma. Parametric simulation studies on Hct clarified the relationships among Hct, RBC deformation and apparent blood flow resistance.

2. Methods

2.1 Particle method for blood flow simulation

In the previous study [12], we proposed a particle method for blood flow simulation to investigate the motion of a single deformable RBC interacting with viscous plasma fluid. In this study, this method was extended to include multiple RBCs. The simulation procedures (1)–(4) are as follows, which are schematically illustrated in Fig. 1. The following equations are written for a two-dimensional problem with unit length in the thickness dimension.

(1) The blood region was discretized by particles that are assumed to have the characteristics of RBCs and plasma, as shown in Fig. 2. It was assumed that an RBC part consists of a surface membrane and inner fluid particles. Each particle i has physical quantities such as the position $\mathbf{r}_i$, velocity $\mathbf{u}_i$, pressure p_i, and constant density ρ.

(2) A spring network model [13] was applied to RBC membrane particles to express the

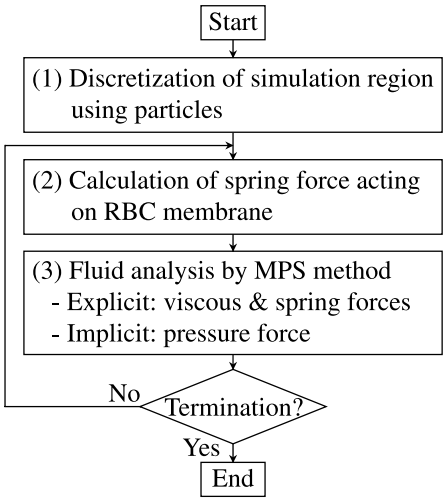

Fig. 1 Algorithm of computer simulation of blood flow using particle method.

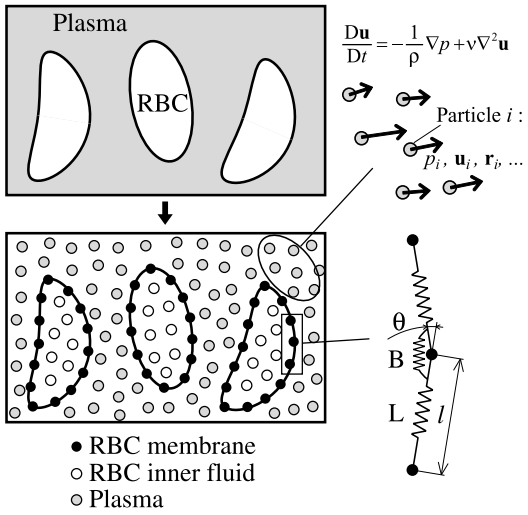

Fig. 2 Discretization of RBCs and plasma using particles. Particle motion was determined on the basis of NS equations using the MPS method. Particles for the RBC membrane were connected by springs to express the membrane's elastic behavior.

elastic behavior of deformable RBCs, in which the membrane particles were connected with the neighboring membrane particles by springs for stretch/compression L and bending B, as shown in Fig. 2. The elastic energy stored in the stretch/compression spring due to the change in the length l from its reference l_0 was expressed as

$$E_l = \frac{k_l}{2}\sum_{I=1}^{N}\left(\frac{l_I - l_0}{l_0}\right)^2 . \quad (1)$$

For bending, the elastic energy can be expressed as a function of the angle θ between two neighboring stretch/compression spring elements. Here, to avoid the folding of spring elements, we determined the elastic energy for bending as

$$E_b = \frac{k_b}{2}\sum_{I=1}^{N}\tan^2\left(\frac{\theta_I}{2}\right). \quad (2)$$

In Eqs. (1) and (2), I is a spring element, N is the total number of spring elements, and k_l and k_b are spring constants for changes in length and bending angle, respectively. Using total elastic spring energy of the RBC membrane,

$$E = E_l + E_b , \quad (3)$$

the elastic spring force acting on the membrane particle i was obtained on the basis of the principle of virtual work as

$$\mathbf{F}_i = -\frac{\partial E}{\partial \mathbf{r}_i} . \quad (4)$$

This force was calculated from position $\mathbf{r}_i$ according to the results of vector analysis.

(3) Assuming incompressible viscous flow, the motion of all the particles was determined under a given boundary condition using the moving particle semi-implicit (MPS) method [14), (15)]. In the MPS method, particle motion is modeled on the basis of the equation of continuity and the Navier-Stokes (NS) equations with a semi-implicit time-marching algorithm. The gradient vectors and Laplacian of the scalar quantity ϕ_i for particle i, which appear in the NS equations, are expressed by considering the interaction to the neighboring particles j as

$$\langle \nabla \phi \rangle_i = \frac{d}{n^0}\sum_{j\neq i}\left[\frac{\phi_j - \phi_i}{|\mathbf{r}_j - \mathbf{r}_i|^2}(\mathbf{r}_j - \mathbf{r}_i)w(|\mathbf{r}_j - \mathbf{r}_i|)\right] \quad (5)$$

and

$$\left\langle \nabla^2 \phi \right\rangle_i = \frac{2d}{n^0 \lambda} \sum_{j \neq i} \left[\left(\phi_j - \phi_i \right) w\left(\left| \mathbf{r}_j - \mathbf{r}_i \right| \right) \right], \tag{6}$$

respectively [15]. In these equations, $w(|\mathbf{r}_j - \mathbf{r}_i|)$ is a kernel function that monotonically decreases with the distance $|\mathbf{r}_j - \mathbf{r}_i|$ between two particles i and j, d is the number of space dimensions, n^0 is the objective value of the number density of particles, and λ is the constant that expresses the increase in the statistical diffusion of the distribution of physical quantities [15]. With respect to RBC membrane particles, the elastic spring force described in Eq. (4) was substituted to the NS equations as the external force term and explicitly solved, which enabled us to perform a coupled analysis of viscous fluid (plasma and inner fluid of RBCs) and an elastic membrane (RBC membrane). Thus, for a membrane particle i a discrete form of the NS equations can be written as

$$\frac{D\mathbf{u}_i}{Dt} = -\frac{1}{\rho} \left\langle \nabla p \right\rangle_i + \left\langle \nabla^2 \mathbf{u} \right\rangle_i + \frac{1}{m_i} \mathbf{F}_i, \tag{7}$$

where m_i is the representative mass of particle i and can be regarded as constant ρd_0^2 with d_0 being the mean distance between two neighboring particles. Equation (7) assumes that membrane particle i can be modeled as an elastic thin membrane surrounded with the fluid in a volume d_0^2.

(4) The procedures (2)–(3) were repeated to obtain the change in blood flow with time.

There are several methods of expressing the elasticity of RBCs in blood flow simulation with a particle method. Boryczko et al. [6] connected all the particles of the RBC part, including both the membrane and inner fluid. Therefore, the inner fluid of an RBC was modeled as an elastic solid but not as a fluid. In another approach, an elastic membrane can be expressed by at least a few layers of elastic particles. However, this method would need an extensive number of particles to discretize the entire simulation region. In this study, the particles of an RBC membrane were modeled by an assembly of particles in one layer and they were explicitly connected by stretch/compression and bending springs. This gives a practical way to simulate the large deformation of RBCs considering the mechanical properties of both the elastic membrane and inner fluid of an RBC.

2.2 Two-dimensional model of blood flow between parallel plates

A two-dimensional simulation model was constructed for blood flow between parallel plates, as shown in Fig. 3. The model consisted of RBCs, plasma and rigid plates. The length of the flow channel L and the distance between the plates D were 90.0 μm and 9.0 μm, respectively. Biconcave RBCs were arranged at equal distances d_{RBC} apart, and their long axes were set perpendicular to the flow direction. The biconcave RBC shape was obtained as the final state of the shape change simulation based on the spring network model [13], the details of which are described in the Appendix. The blood flow models were constructed for various Hct values from 0.10 to 0.49 by adjusting the distance d_{RBC} between RBCs from 22.0 μm to 4.5μm.

As a boundary condition, a constant and uniform velocity $u_0 = 1.1 \times 10^{-2}$ m/s was

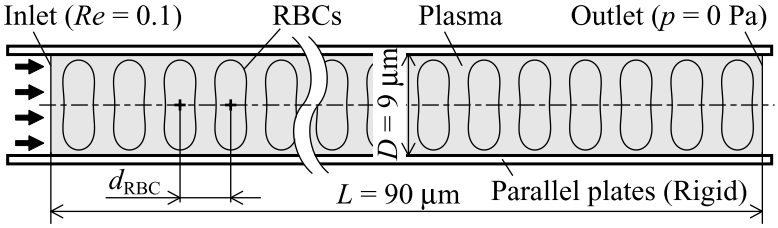

Fig. 3 Two-dimensional model of blood flow between parallel plates. Biconcave RBCs were placed with various distances d_{RBC} to adjust Hct values from 0.10 to 0.49.

applied to the inlet, where the Reynolds number with respect to the plate separation distance D was 0.10. Inflow of RBCs was intermittent, and the interval of RBC inflow was determined from the Hct value. A zero-pressure condition was applied to the outlet. A nonslip condition was assumed between the plasma and the RBC, and between the plasma and the plates. The viscosity and density were 1.0×10^{-3} Pa·s and 1.0×10^{3} kg/m^3, respectively, set to be the same as those of water. The mean distance between two neighboring discrete particles was set to 0.25 μm, and thus the simulation area contained approximately 15000 particles. The spring constants of the RBC membrane were set as $k_l = 5.0\times10^{-8}$ N·m in Eq. (1) for stretch/compression, and $k_b = 5.0\times10^{-10}$ N·m in Eq. (2) for bending (see the Appendix for spring constant values). The reference length of the stretch spring was l_0 = 0.25 μm , the same as the mean distance between two neighboring particles.

3. Results and Discussion

3.1 RBC deformation and movement

The dynamical behavior of elastic RBCs in flowing blood between parallel plates was investigated by computer simulation. Figure 4 shows the characteristic movement and deformation of RBCs in blood flow in the case of Hct = 0.49. The simulation time t is normalized by the time $T_0 = L/u_0$. The RBCs moved downstream in the flowing plasma at a constant velocity. At the onset of the flow (t/T_0 = 0 and 0.10), the RBCs maintained their concave shape at the upstream and were deformed into a convex shape at the downstream, similar to the parachute shape observed in experiments [2]. From t/T_0 = 0.30 to 0.60, the RBCs were kept deformed into a parachute shape, and the blood flow reached a steady state.

Figure 5 shows the mechanical behavior of RBCs in blood flow at time t/T_0 = 1.0 for various Hct values from 0.10 to 0.49. This parametric study on Hct demonstrated that at higher Hct, RBCs were less deformed. The degree of deformation of RBCs was quantified by a deformation index $\varepsilon = |(h - h_0)/h_0|$, where h and h_0 are the projection length of an RBC against the cross section of the flow channel and its initial value, respectively, as shown in Fig. 6. This figure shows the time course of the change in the mean value of the deformation index, ε_M, in the middle part of the flow channel with a length of $L/3$ indicated by the dotted box in Fig. 5. Deformation index ε_M monotonically increased for all the

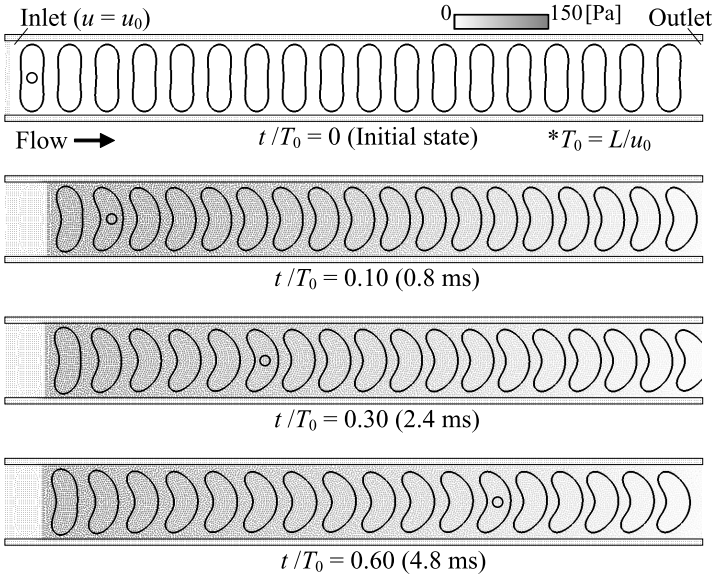

Fig. 4 Simulation results of time course of change in RBC behavior in blood flow in the case of Hct = 0.49. The open-circle marker inside an RBC indicates the same RBC at a different time.

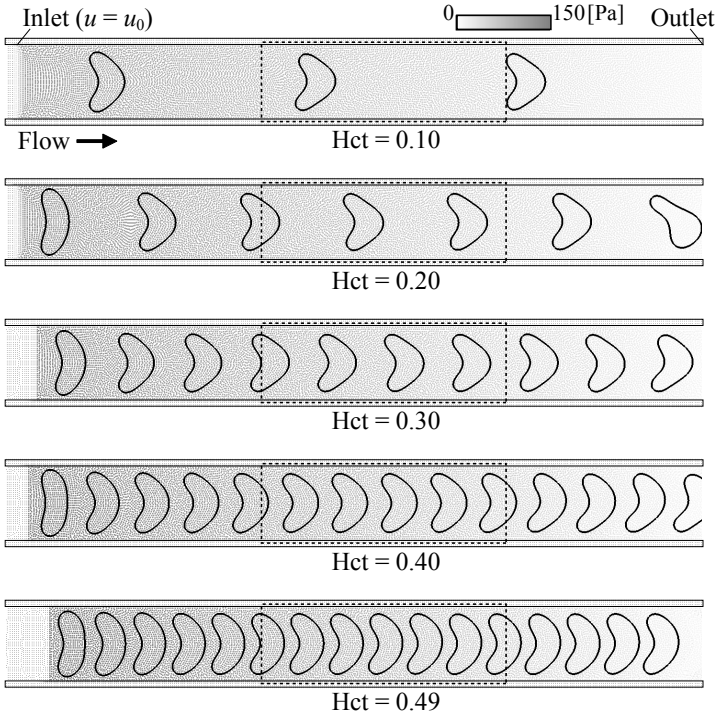

Fig. 5 RBC behavior in blood flow at normalized time $t/T_0 = 1.0$ for various Hct values from 0.10 to 0.49. The middle part of the flow channel with a length of $3/L$ indicated by a dotted box is used to evaluate apparent flow properties in Figs. 6, 7, 11 and 12.

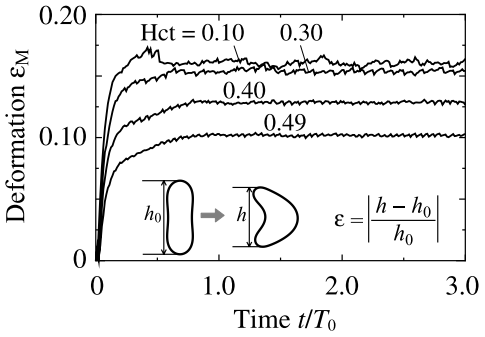

Fig. 6 Change in deformation index of RBCs in middle part of flow channel for various Hct values.

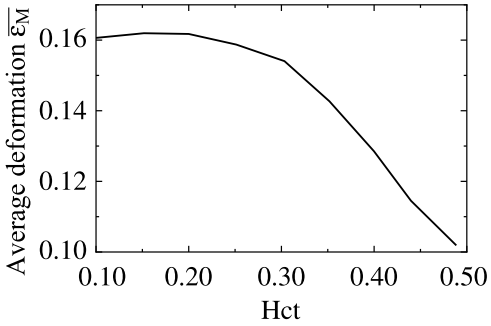

Fig. 7 Mean value of deformation index over time from time $t/T_0 = 1.0$ to 3.0 as function of Hct.

values of Hct, and remained constant from time $t/T_0 = 1.0$ to 3.0, although the value was fluctuated due to the numerical instability of the particle method and the intermittent inflow condition of RBCs. Figure 7 shows the mean value of the deformation index over the time from $t/T_0 = 1.0$ to 3.0, $\overline{\varepsilon_M}$, as a function of Hct. Average deformation index $\overline{\varepsilon_M}$ remained constant when Hct was smaller than 0.20, and monotonically decreased with increasing Hct. The deformation index $\overline{\varepsilon_M}$ for Hct = 0.49 was smaller by 37% than Hct = 0.10. The result agrees with the suppressing effects of Hct on RBC deformation observed in *in vitro* experiments [16].

Previous experimental work suggests that high Hct in tubes greater than 7 μm can cause transition of RBC flow from single-file with parachute shapes to multi-file with slipper shapes [2]. At high Hct in our simulations multi-file flow was not predicted. This could be because the initial RBC arrangement in our simulation was set to straight single-file. The mulit-file flow observed experimentally could be explained by an initial random

arrangement. Thus future work is necessary to test the effects of initial RBC arrangement and the causes of single- to mulit-flow transitions.

3.2 Mechanical interaction among RBCs and plasma

Figure 8 shows the fluid force acting on an RBC membrane in the cases of Hct = 0.10, 0.30 and 0.49. Arrows on RBCs shown in Fig. 8 illustrate the fluid force vectors per the unit length on the membrane, $\mathbf{f}_{\mathrm{Fluid}}^{\mathrm{RBC}}$ [N/m], that were calculated from the viscous and pressure force terms in NS equations. The force $\mathbf{f}_{\mathrm{Fluid}}^{\mathrm{RBC}}$ is normalized by the stretch/compression spring constant k_l and the reference length of the membrane element, l_0, introduced into the elastic RBC model as $\mathbf{f}_{\mathrm{Fluid}}^{\mathrm{RBC}} l_0 / (k_l / l_0) = \mathbf{f}_{\mathrm{Fluid}}^{\mathrm{RBC}} l_0^{\,2} / k_l$. The force vectors were tangential to the RBC membrane in the vicinity of the parallel walls, as shown by closed circles in Fig. 8. This indicates that the viscous drag force was generated by the difference in velocity between the fixed parallel walls and the RBC. Approaching the central region of the flow channel, force vectors became normal to the RBC membrane, as shown by closed squares in Fig. 8. The normal force vectors indicate that the pressure force is dominant in the fluid force on the RBC membrane. Figure 9 shows the magnitude of the fluid force, $F_{\mathrm{Fluid}}^{\mathrm{RBC}} l_0^{\,2} / k_l$, acting on the RBC membrane as a function of Hct.

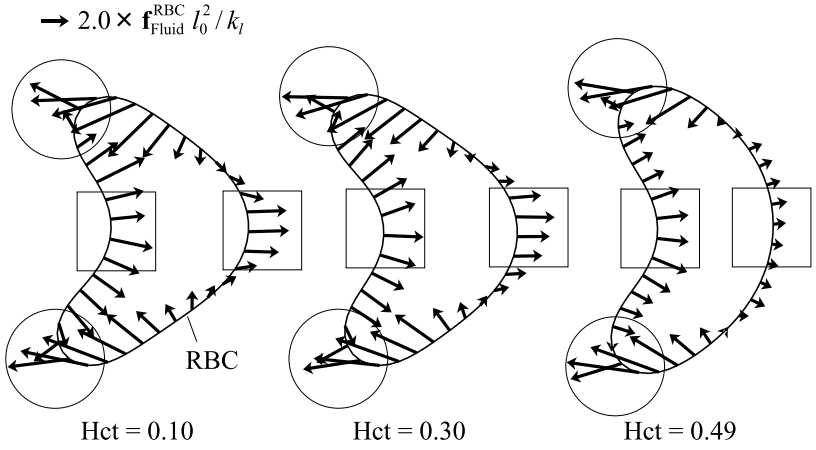

Fig. 8 Fluid force $\mathbf{f}_{\mathrm{Fluid}}^{\mathrm{RBC}} l_0$ acting on RBC membrane for Hct values of 0.10, 0.30 and 0.49. The force is normalized by stretch/compression spring constant k_l and the reference length, l_0, of the stretch spring as $\mathbf{f}_{\mathrm{Fluid}}^{\mathrm{RBC}} l_0^{\,2} / k_l$. The length of an arrow indicates the magnitude of the normalized force.

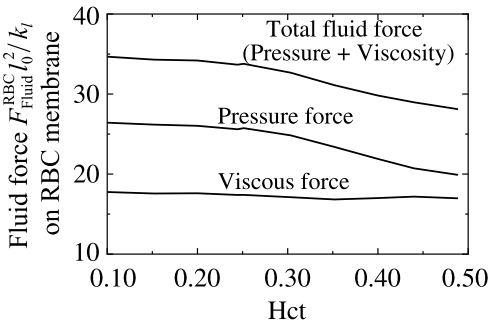

Fig. 9 Magnitude of fluid force, $F_{\mathrm{Fluid}}^{\mathrm{RBC}} l_0^{\,2} / k_l$, acting on RBC membrane as function of Hct. The definition of $F_{\mathrm{Fluid}}^{\mathrm{RBC}}$ is explained in Sec. 3.2. The magnitude of the force $F_{\mathrm{Fluid}}^{\mathrm{RBC}} l_0^{\,2} / k_l$ is illustrated for pressure force, viscous force, and total fluid force (sum of pressure and viscous forces).

$F_{\text{Fluid}}^{\text{RBC}}$ [N/m] was defined as

$$F_{\text{Fluid}}^{\text{RBC}} = \sqrt{\frac{\int_{l_a} \left| \mathbf{f}_{\text{Fluid}}^{\text{RBC}} \right|^2 dl}{l_a}}, \tag{8}$$

where l_a [m] is the total peripheral length of the RBC membrane. The magnitude of the total fluid force (sum of pressure and viscous forces) increased with decreasing Hct. This was due to an increase in pressure force with decreasing Hct, whereas viscous force did not change with Hct, as shown in Fig. 9. The total fluid force remained constant when Hct was smaller than around 0.20.

The dependence of the fluid force acting on the RBC membrane on Hct was associated with fluid flow. Figure 10 shows the velocity vectors of the flow of plasma and the inner fluid of an RBC (left) in the cases of Hct = 0.10, 0.30 and 0.49, and their components on the axial direction of the flow channel as a function of y coordinate, which is set perpendicular to the axial direction (right). This graph demonstrates that at lower Hct, the axial velocity of plasma was spatially more distributed in the central region of the flow channel. Comparing the distribution of plasma flow around an RBC (Fig. 10) and the fluid force acting on the RBC (Fig. 8), it was suggested that the velocity distribution of plasma flow caused the force distribution acting on the RBC membrane, and that this fluid force distribution enhanced RBC deformation into a parachute shape. The velocity profile of the inner fluid of the RBC was flat, demonstrating that the velocity of the inner fluid was not spatially distributed and was the same as that of the RBC membrane because the inner fluid flow was restricted by its surrounding RBC membrane. In the high-Hct cases, the velocity profile of plasma was flat because the plasma fluid was packed in between the neighboring RBCs and its flow was restricted, similar to the mechanism of the restriction of the RBC inner fluid flow by the RBC membrane. On the other hand, the flat velocity profile did not generate the distribution of the fluid force acting on the RBC membrane, resulting in restriction of RBC deformation. This indicates that both the effects of plasma on RBCs and vice versa worked to restrict RBC deformation in high-Hct cases.

Both the degree of RBC deformation (Fig. 7) and the magnitude of the fluid force acting on RBC membrane (Fig. 9) as a function of Hct did not change when Hct values were less than 0.20～0.30, in which case the distance between RBCs was more than 7.0～11.0. When the Hct values were less than 0.20～0.30, the plasma flow profiles obtained by simulation were the same as the flow profiles of plasma without RBCs when the distance between plasma and RBCs ranged from $2/D$ (= 4.5 μm) to D (= 9.0 μm). These results demonstrate that mechanical interaction between RBCs has a significant influence on RBC deformation and plasma flow properties when the Hct values are more than 0.20～0.30, in which the distance between RBCs is within the size of an RBC.

3.3 Blood flow resistance

Figure 11 shows the time course of the change in apparent pressure drop Δp in the middle part of the flow channel. In this graph, pressure drop Δp is normalized by the pressure drop $(\Delta p)_0$ of plasma flow without RBCs. Pressure drop $\Delta p/(\Delta p)_0$ increased at the onset of flow, and gradually decreased until time t/T_0 = 1.0. After that, pressure drop $\Delta p/(\Delta p)_0$ converged to a constant value. The solid line in Fig. 12 shows the mean value of the pressure drop over the time from t/T_0 = 1.0 to 3.0, $\overline{\Delta p}/(\Delta p)_0$, as a function of Hct. Average pressure drop $\overline{\Delta p}/(\Delta p)_0$ monotonically increased from 1.02 to 1.36 with increasing Hct from 0.10 to 0.49. This result is consistent with previously reported results of *in vitro* experiments compiled to an empirical formula [(1), (4)], as shown by a dotted line, in which the difference in pressure drop $\overline{\Delta p}/(\Delta p)_0$ between the simulation and *in vitro* experiments was less than 2.2%.

The blood flow resistance obtained by simulation as a function of Hct qualitatively

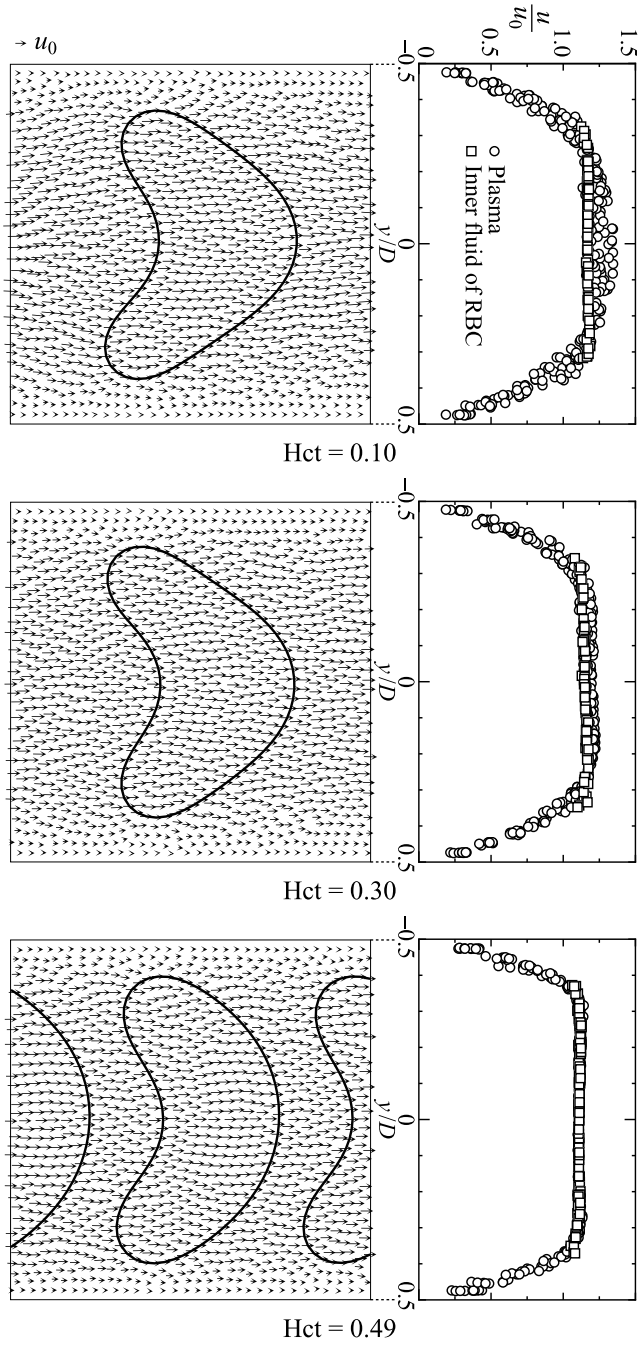

Fig. 10 Velocity vectors of plasma around RBC (left) and their components in axial direction of flow channel (right) for Hct values of 0.10, 0.30 and 0.49. The magnitude of velocity is normalized by the inlet velocity value u_0 on the right. The focus of interest is the square region with D = 9.0 μm on each side in the middle part of the flow channel.

agrees with *in vitro* experimental results using a micro flow channel [4]. The difference of 2.2% between the simulation and experiments might indicate the quantitative correspondence between simulation and experiments. However, the simulation result is two dimensional, whereas the experimental results are three dimensional. In addition, model parameters introduced in RBCs, such as membrane spring constants and the viscosity of inner fluid, were determined to express both the RBC deformation into parachute shape and the apparent flow resistance expressed by an empirical formula. Therefore, it is an important future work to compare the results of a three-dimensional simulation with experimental results,

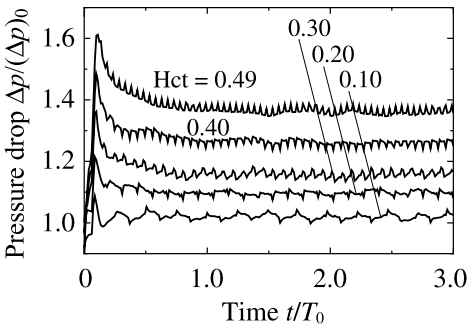

Fig. 11 Change in apparent pressure drop in middle part of flow channel for various Hct values. Pressure drop Δp in the longitudinal axis is normalized by pressure drop $(\Delta p)_0$ in the case of plasma flow without RBCs.

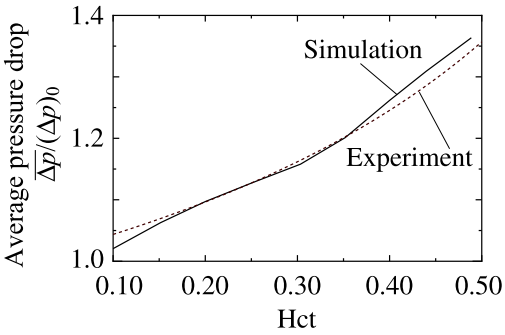

Fig. 12 Mean value of pressure drop over time from $t/T_0 = 1.0$ to 3.0 as function of Hct. Solid and dotted lines show the results of the simulation and *in vitro* experiments complied to an empirical formula [1), (4)], respectively.

which will provide us a quantitative evaluation of the relationships of mechanical behaviors in microcirculation between blood components and the resulting rheology of blood.

4. Conclusions

A two-dimensional computer simulation of blood flow was carried out using a particle method to consider the mechanical behaviors of deformable multiple RBCs. Simulation results demonstrated a suppressing effect of Hct on RBC deformation into a parachute shape. This was associated with the fluid force acting on an RBC, which was determined by the mechanical interaction among RBCs and plasma. The mechanical interaction determined RBC deformation and plasma flow properties, determining blood flow resistance as a function of Hct.

Acknowledgments

The authors thank Prof. Seiichi Koshizuka of the University of Tokyo for providing the source code of the basic part of the MPS method. They are also grateful to Prof. Ryo Kobayashi of Hiroshima University for helpful comments on the elastic RBC membrane model. This work was supported by the following grants; Grants in Aid for Scientific Research by the Ministry of Education, Culture, Sports, Science and Technology (MEXT) of Japan (Scientific Research (A) (16200031) and Scientific Research in Priority Areas (768)). "Revolutionary Simulation Sofrware (RSS21)" project of next generation of IT program of MEXT. The first author was financially supported in part by MEXT Overseas Advanced Educational Research Practice Support Program, Support Projects in the New Fields of Interdisciplinary Research Creation.

Appendix

The shape change of a swollen RBC was simulated on the basis of the spring network model [13], as shown in Fig. 13. As an initial state, the RBC was assumed to have a circular shape with a diameter of $\Phi = 6.0$ μm. The circular RBC was discretized into $N = 76$ RBC membrane particles that were connected by stretch/compression and bending springs with the neighboring particles, as denoted in Sec. 2.1. The RBC membrane particles moved so that the total elastic energy became minimum by solving a set of motion equations for each particle,

$$m\ddot{\mathbf{r}}_i + \gamma\dot{\mathbf{r}}_i = \mathbf{F}_i, \tag{9}$$

by the finite difference method (FDM). Here, a dot $\dot{(\ )}$ denotes the time derivative, and m and γ are the representative mass and viscosity of the RBC, respectively. Force $\mathbf{F}_i$ due

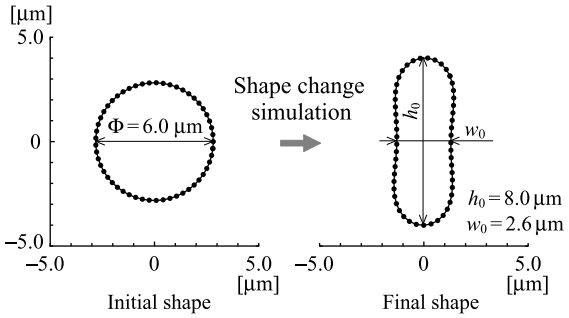

Fig. 13 Shape change simulation of swollen RBC due to volumetric reduction using spring network model based on minimum energy principle. An initial circular RBC changed to have a biconcave shape at the final state of the simulation.

to total elastic spring energy E is expressed as

$$\mathbf{F}_i = -\frac{\partial(E+\Gamma_s)}{\partial \mathbf{r}_i}, \tag{10}$$

instead of Eq. (4) in order to introduce an areal constraint with penalty function Γ_s. This penalty function was defined as

$$\Gamma_s = \frac{k_s}{2}\left(\frac{s-s_0}{s_0}\right)^2, \tag{11}$$

where s and s_0 are the RBC area and its reference value, respectively. The spring constants in Eqs. (1) and (2) were set to have the same values as those used in Sec. 2.3. The other parameters were set as follows; the mass $m = 2.0\times10^{-4}$ μg and viscosity $\gamma = 1.0\times10^{-2}$ N·s/m in Eq. (9), and the penalty coefficient $k_s = 1.0\times10^{-5}$ N·m in Eq. (11). As a result of shape change simulation in the case of volumetric reduction to 70% of the initial circular shape (that is, reference volume s_0 was set to 70% of the initial shape), a biconcave RBC was obtained at the final state. The size of the biconcave RBC was h_0 = 8.0 μm in axial length and w_0 = 2.6 μm in the thickness of the concave part. This biconcave shape corresponds to that observed in a normal RBC.

Spring constants k_l and k_b in Eqs. (1) and (2) determine the elastic properties of RBC membrane in the blood flow simulation. The bending constant, k_b, can be reduced to a bending stiffness coefficient B of the membrane by comparing bending elastic energy E_b in Eq. (2) with the analytical solution E_b' calculated by coefficient B and membrane curvature C [13]. Assuming a two-dimensional circular shape of RBC membrane as shown in the left side of Fig. 13, the bending energy E_b' is calculated by line integrals along the circumference $L = \pi\phi$ with the constant curvature $C = 1/(\phi/2)$,

$$E_b' = \frac{1}{2}B\int_L C^2 dl = \frac{1}{2}B\int_0^{\pi\phi}\left(\frac{1}{\phi/2}\right)^2 dl = \frac{2B\pi}{\phi}. \tag{12}$$

Based on previous reported constant B values ($B = 0.4\sim3.0\times10^{-19}$ N·m)[17], $k_b = 0.6\sim4.8\times10^{-12}$ N·m. In a preliminary calculation, however, these values of k_b resulted in excessive deformation of RBC in a two-dimensional blood flow simulation. This is due to the fact that a membrane structure in two-dimensional problem is more easily deformed than that with three-dimensional shape. Therefore, the constant k_b was set approximately a hundredfold in this study to compensate for the decreased stiffness of the membrane in two-dimensional problem and to express realistic RBC deformation. In our two-dimensional simulations this adjustment resulted in RBC deformation and pressure drop comparable to real three-dimensional cases. Stretch/compression constant k_l in two-dimensional problem represents both planar shear deformation and incompressibility of membrane in three-dimensional one. The value of the constant k_l in this study was chosen to ensure that RBCs in no flow state have a biconcave shape which is determined by the ratio of k_l to k_b.

Nomenclature for Normalized Values

Hematocrit values:	Hct
Reynolds number:	$\mathrm{Re} = u_0 D/\nu$
Normalized simulation time:	$t/T_0 \quad (T_0 = L/u_0)$
Deformation index:	$\varepsilon = \lvert(h - h_0)/h_0\rvert$
Time average of deformation index:	$\overline{\varepsilon_{\mathrm{M}}}$
Normalized fluid force acting on RBC membrane:	$\mathbf{f}_{\mathrm{Fluid}}^{\mathrm{RBC}} l_0^{\,2}/k_l$
Magnitude of normalized fluid force acting on RBC:	$F_{\mathrm{Fluid}}^{\mathrm{RBC}} l_0^{\,2}/k_l$
Normalized pressure drop:	$\Delta p/(\Delta p)_0$
Time average of normalized pressure drop:	$\overline{\Delta p}/(\Delta p)_0$

References

(1) Pries, A.R., et al., Biophysical Aspects of Blood Flow in the Microvasculature, *Cardiovascular Research*, Vol. 32, No. 4 (1996), pp. 654-667.

(2) Sugihara-Seki, M. and Fu, B. M., Blood Flow and Permeability in Microvessels, *Fluid Dynamics Research*, Vol. 37, No. 1/2 (2005), pp. 82-132.

(3) Baskurt, O. K. and Meiselman, H. J., Blood Rheology and Hemodynamics, *Seminars in Thrombosis and Hemostasis*, Vol. 29, No. 5 (2003), pp. 435-450.

(4) Pries, A.R., et al., Redistribution of Red Blood Cell Flow in Microcirculatory Networks by Hemodilution, *Circulation Research*, Vol. 70, No. 6 (1992), pp. 1113-1121.

(5) Sun, C. and Munn, L. L., Particulate Nature of Blood Determines Macroscopic Rheology: A 2-D Lattice Boltzmann Analysis, *Biophysical Journal*, Vol. 88, No. 3 (2005), pp. 1635-1645.

(6) Boryczko, K., et al., Dynamical Clustering of Red Blood Cells in Capillary Vessels, *Journal of Molecular Modeling*, Vol. 9, No. 1 (2003), pp. 16-33.

(7) Monaghan, J. J., Smoothed Particle Hydrodynamics, *Reports on Progress in Physics*, Vol. 68, No. 8 (2005), pp. 1703-1759.

(8) Boryczko, K., et al., Modeling Fibrin Aggregation in Blood Flow with Discrete-Particles, *Computer Methods and Programs in Biomedicine*, Vol. 75, No. 3 (2004), pp. 181-194.

(9) Takano, T. et al., Micro-Simulation of Blood Flow, *Transactions of the Japan Society of Mechanical Engineers, Series B*, Vol. 70, No. 699 (2004), pp. 2705-2711.

(10) Kamada, H., et al., Computer Simulation of Formation and Collapse of Primary Thrombus due to Platelet Aggregation Using Particle Method, *Transactions of the Japan Society of Mechanical Engineers, Series B*, Vol. 72, No. 717 (2006), pp. 1109-1115.

(11) Tsubota, K., et al., Simulation Study on Effects of Deformabilities of Red Blood Cells on Blood Flow Using Particle Method, *Transactions of the Japan Society of Mechanical Engineers, Series B*, Vol. 72, No. 718 (2006), pp. 1483-1489.

(12) Tsubota, K., et al., Particle Method for Computer Simulation of Red Blood Cell Motion in Blood Flow, *Computer Methods and Programs in Biomedicine*, Vol. 83, No. 2, (2006), pp. 139-146.

(13) Wada, S. and Kobayashi, R., Numerical Simulation of Various Shape Changes of a Swollen Red Blood Cell by Decrease of its Volume, *Transactions of the Japan Society of Mechanical Engineers, Series A*, Vol. 69, No. 699 (2003), pp. 14-21.

(14) Koshizuka, S. and Oka, Y., A Particle Method for Incompressible Viscous Flow with Fluid Fragmentation, *Computational Fluid Dynamics Journal*, Vol. 4, No. 1 (1995), pp. 29-46.

(15) Koshizuka, S. and Oka, Y., Moving-Particle Semi-Implicit Method for Fragmentation of Incompressible Fluid, *Nuclear Science and Engineering*, Vol. 123, No. 3 (1996), pp. 421-434.

(16) Kon, K., et al., Erythrocyte Deformation in Shear Flow: Influences of Internal Viscosity, Membrane Stiffness, and Hematocrit, *Blood*, Vol. 69, No. 3 (1987), pp. 727-734.

(17) Hochmuth, R. M. and Waugh, R. E., Erythrocyte Membrane Elasticity and Viscosity, *Annual Review of Physiology*, Vol. 49 (1987), pp. 209-219.